



Andreas Weber

Planning, Construction and Commissioning of a Stretched Hollow Core Fiber Pulse Compressor

BACHELOR THESIS

to achieve the university degree of Bachelor of Science Bachelor's degree programme: Physics

submitted to

Graz University of Technology

Supervisor

Marcus Ossiander, Ass.Prof. Dr.rer.nat. B.Sc. M.Sc. Institute for Experimental Physics

Affidavit

-	dently, that I have not used other than the declared licated all material which has been quoted either
	The text document uploaded to tugrazonline is
identical to the present bachelor thesis.	1 8
Date	Andreas Weber

Acknowledgments

To begin with, I would like to extend my sincere thanks to my supervisor Ass. Prof. Marcus Ossiander for continuous support throughout my thesis project and making me really feel part of his research group. He spent countless hours with me in laboratory teaching me important skills like beam walking, leak testing of a pressure vessel and much more. Moreover, I am really grateful for the support provided by Dipl.-Ing. Hana Hampel, who helped me with a lot of laboratory work and gave me really valuable advice during the construction process. Additionally, I would like to thank Dipl.-Ing. Alexander Grossek for sharing his workspace with me and for always providing a helping hand. Finally, but certainly not least special thanks are due to the workshop at Graz University of Technology, which produced numerous components for me, no matter of how complicated they were to manufacture.

Abstract

The development of high-intensity lasers pulses containing only a few optical cycles has become critical for modern scientific applications, particularly in strong-field and attosecond physics. Achieving such short pulse durations often requires nonlinear pulse compression techniques due to the limited gain bandwidth of the lasers themselves. The most common approach utilizes the optical Kerr effect for spectral broadening via self-phase modulation (SPM). Subsequently managing the dispersion of the broadened laser pulses then yields temporal compression.

This thesis presents the design, construction, and commissioning of a stretched hollow core fiber pulse compressor, encapsulated by a pressure vessel. When filled with 21 bar of Neon gas, the 1.1 m long hollow core fiber broadens the spectrum of a commercial Yb:KGW laser from approximately 20 nm to 330 nm with a transmission of up to 55%. This corresponds to a decrease of the Fourier limited pulse duration from 150 fs to <9 fs.

Contents

1	Intr	oduction	6
2	The	ory of Spectral Broadening	7
	2.1	Gaussian Laser Pulses	7
	2.2	Pulse Duration and Spectral Bandwidth	8
	2.3	Self-Phase-Modulation	8
	2.4	Achieving Large Spectral Broadening	11
3	Con	npressor Construction	12
	3.1	Used Fibers	12
	3.2	Cutting the Fiber	12
	3.3	Mounting the Fiber	13
	3.4	Fiber Coupling Tests (HeNe-Laser)	15
	3.5	Pressure Vessel	16
4	Con	npressor Commissioning	18
	4.1	Results Fiber I	20
	4.2	Results Fiber II	21
5	Disc	ussion and Outlook	23

1 Introduction

Since their conception, by Albert Einstein, many different lasers (light amplification by stimulated emission of radiation) for a wide field of applications reaching from medical usage to measurement devices were developed. Relatively new and up to date applications for lasers are strong field and attosecond science, especially with respect to the Nobel Prize for Anne L'Huillier, Pierre Agostini and Ferenc Krausz. In this field high intensity lasers with extremely short pulse durations are indispensable. To achieve such pulses, laser pulses emitted from the system are temporally compressed by nonlinear pulse compressors which add frequency components to the laser spectrum. The reason for this is the intensity dependent part of the refractive index. By aligning the phase relation between the generated frequencies with e.g. chirped mirrors, the laser pulse can be compressed.

A Yb:KGW semiconductor laser, which uses ytterbium doped potassium gadolinium tungstate as laser medium, was used to test the functionality of a stretched hollow core fiber pulse compressor which was planned and built in the course of this thesis. The laser generates pulses with a duration of around 150 fs with a central wavelength of 1030 nm. The compressor consists of a pressure vessel filled with Neon gas at pressures of around 20 bar. Inside this vessel is a stretched hollow core fused silica fiber, into which the laser was focused. During propagation through the gas, the laser undergoes self-phase modulation. Therefore, in theory, a completely different spectrum should be measured if the laser intensity and gas pressure are high enough. Special motivation to build this type of pulse compressor is large a flexibility in terms of fiber length, nonlinear medium and input pulse energy.

2 Theory of Spectral Broadening

The following chapter briefly introduces the theoretical background of ultrashort laser pulses and nonlinear spectral broadening.

2.1 Gaussian Laser Pulses

The most common treatment of ultrashort laser pulses assumes a temporally oscillating electric field under a Gaussian envelope. Figure 1 shows an example. Mathematically, the real electric field E(t) of a compressed pulse is described by an oscillating term multiplied with a Gaussian function, e.g.:

$$E(t) = E_0 \cdot \operatorname{Re}\left(e^{i\omega_0 t}\right) \cdot \mathcal{E}(t) \text{ with } \mathcal{E}(t) = e^{-2\log(2)\left(\frac{t}{\tau}\right)^2}$$
(1)

Here, E_0 represents the amplitude of the electric field, ω_0 the central angular frequency, t the time, and τ measures the duration of the pulse. The above formulation is chosen such that the pulse duration τ is the full with at half maximum (FWHM) of the time-domain intensity envelope I(t), which is proportional to the square of the electric field envelope $\mathcal{E}(t)$. [2, p. 2-5]

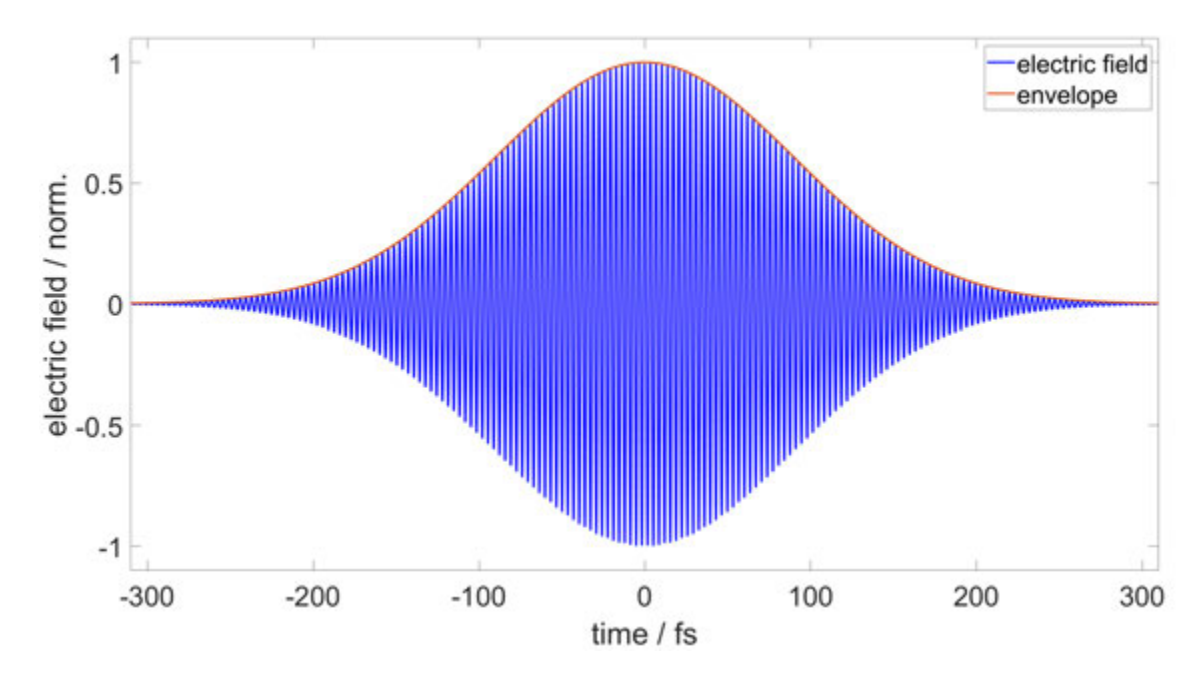


Figure 1: The electric field of a Gaussian laser pulse and its envelope. The parameters are set to about $E_0=1\frac{\rm V}{\rm m}$, $\omega=291$ THz, $\tau=150$ fs

2.2 Pulse Duration and Spectral Bandwidth

Frequency and time domain are connected via the Fourier transform, therefore, it is possible to describe the same ultrashort pulse as an angular-frequency-dependent complex electric field $\tilde{E}(\omega)$:

$$\tilde{E}(\omega) = \mathcal{F}\{E(t)\} = \int_{-\infty}^{\infty} E(t)e^{-i\omega t}dt$$
 (2)

Given $\tilde{E}(\omega)$, the time-dependent electric field can be obtained using the inverse Fourier transform: [9, p. 5]

$$E(t) = \mathcal{F}^{-1}\{\tilde{E}(\omega)\} = \frac{1}{2\pi} \int_{-\infty}^{\infty} \tilde{E}(\omega) e^{i\omega t} d\omega.$$
 (3)

However, e.g., a spectrometer only measures the spectral intensity, i.e., the absolute square of the spectral amplitude $|\tilde{E}(\omega)|^2$, not its phase. Whereas the measured spectrum does not reveal a light pulse's actual duration, it provides a limit for the minimal duration to which the light pulse can be compressed. Using the spectral width $\Delta\omega$, defined as the FWHM of the spectral intensity $|\tilde{E}(\omega)|^2$, the bandwidth theorem states that the product of the spectral width and pulse duration can not be smaller than a constant defined by the pulse shape: [9, p. 9]

$$\tau \cdot \Delta \omega \ge \text{const.}$$
 (4)

As can be seen directly from this relation, a broader spectral width supports shorter pulse durations. For any spectrum, the minimum pulse duration is limited by the equality. For this to occur, all spectral components of a pulse must be perfectly in phase at some point in time, i.e., the spectral phase, $arg(\tilde{E(\omega)})$, must be linear. A pulse with this property is called a Fourier transform limited pulse. [7]

Because most lasers have a too narrow spectrum to create pulses with single-digit femtosecond durations, achieving such durations requires broadening their spectrum.

2.3 Self-Phase-Modulation

One way to increase an ultrashort pulse's bandwidth is the nonlinear interaction of light with matter. At high intensities I(t), the Kerr effect adds an intensity-dependent term to the refractive index n(t) of a medium, also rendering it time-dependent:

$$n(t) = n_0 + n_2 \cdot I(t) \tag{5}$$

Here, n_0 represents the linear refractive index and n_2 the second order nonlinear refractive index. [7] The origin of this effect can be explained by the binding potential of electrons in matter, see Figure 2: For small displacements, the binding potential can be described as harmonic (parabolic) potential, i.e., electrons displaced by a small amount from their equilibrium position experience a restoring force that linearly increases with their displacement. A consequence is that electrons subjected to an externally applied oscillating electric field (a light pulse) also oscillate with the frequency of the applied field. This causes a time-varying polarization in the medium which is the origin of the refractive index. For larger displacements, the binding potential becomes anharmonic, i.e., it must be described using higher order terms, and the restoring force becomes nonlinear. Thus, also the movement of the electron in reaction to an external electric field becomes nonlinear, the polarization becomes nonlinear, and thus the refractive index becomes nonlinear. If the binding potential is symmetric around the equilibrium position of the electron, the first non-zero higher order term is n_2 . [7]

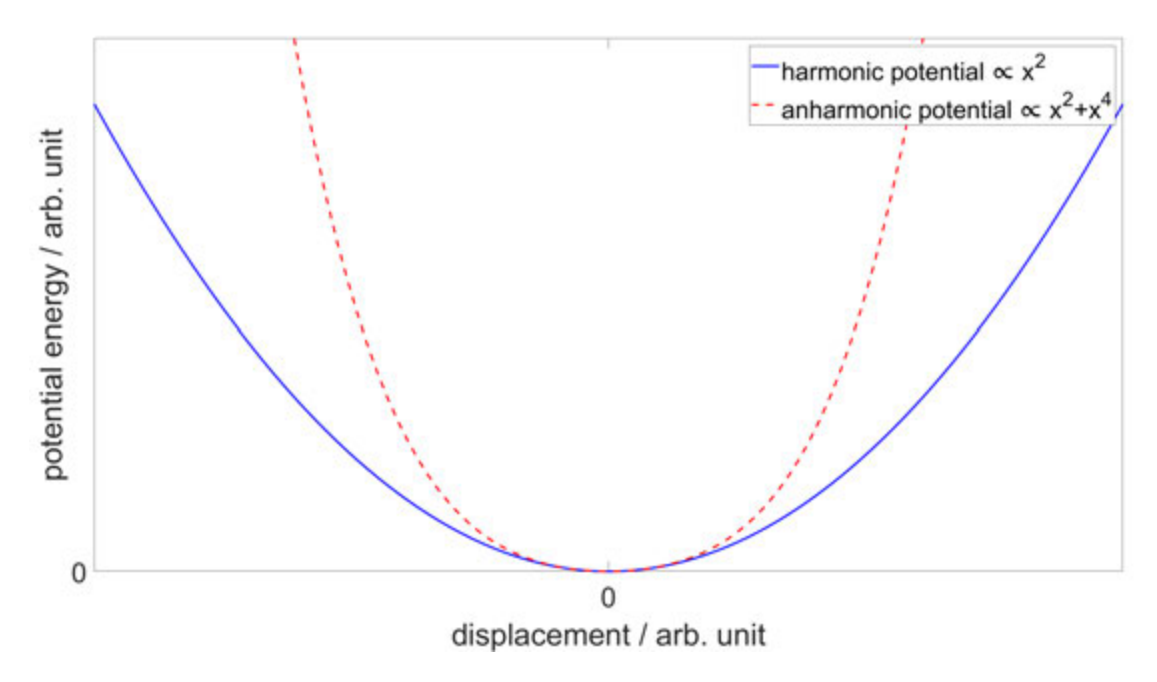


Figure 2: The harmonic potential can be used to approximate a harmonic potential containing higher order terms in the region around the minimum of the potential. For increasing displacement, they start to differ.

When a light pulse propagates through a medium described by a refractive index following Equation 5, it can modulate its own temporal phase and create new frequencies: We start with a plane wave that travels along the x-direction in a nonlinear Kerr medium:

$$E(t,x) = E_0 e^{i(\omega_0 t - kx)} = E_0 e^{i\Phi(t)}, \quad k = \frac{2\pi}{\lambda_0} n(t) = \frac{\omega_0}{c_0} n(t)$$
 (6)

Where k is the light field's wave number which is related to its vacuum wavelength λ_0 by the medium's refractive index and to the angular frequency by the speed of light in vacuum c_0 . The time derivative of the light pulse's temporal phase $\Phi(t)$ gives its instantaneous frequency $\omega_{inst}(t)$:

$$\omega_{inst}(t) = \frac{\partial}{\partial t} \Phi(t) = \omega_0 - \frac{\omega_0}{c_0} \frac{\partial n(t)}{\partial t} x \tag{7}$$

After propagating a distance x in the nonlinear medium, the instantaneous frequency depends on the light intensity, with a frequency variation $\delta\omega(t)$ of:

$$\delta\omega(t) = \omega_{inst}(t) - \omega_0 = -\frac{\omega_0 n_2}{c_0} x \frac{\partial I(t)}{\partial t}$$
(8)

As the laser pulse's instantaneous frequency, and connected to it its phase, depends on its own intensity, this process is called self-phase modulation (SPM).

Starting with a compressed light pulse with an envelope as in Equation 1, leads to a time-varying intensity envelope. If the nonlinear refractive index is positive, the leading edge of the pulse envelope generates lower frequencies (broadens the red side of the spectrum), while the trailing edge produces higher frequencies (broadens the blue side). Figure 3 visualizes this behavior. The maximal spectral shifts are reached for the highest slopes of the intensity envelope. [7]

Additional frequencies are generated within the bounds of the pulse's temporal envelope but are not phase-synchronized. Thus, the pulse is no longer transform-limited as it propagates through

the medium. Figure 4 shows the self phase modulated electric field from Figure 1.

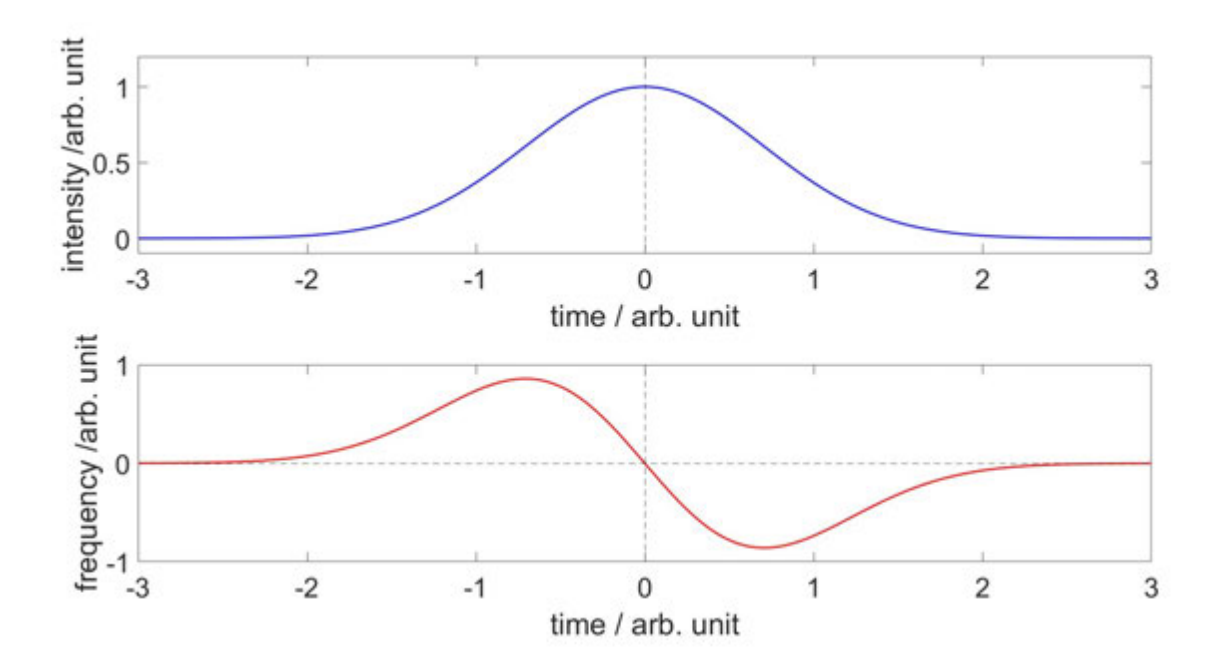


Figure 3: The intensity envelope of a Gaussian pulse (upper graph) undergoes a self-frequency (lower graph) shift due to SPM when traveling through a nonlinear medium. The leading edge (time) of the pulse broadens the side with lower frequencies and the trailing edge (time) the side with higher frequencies.

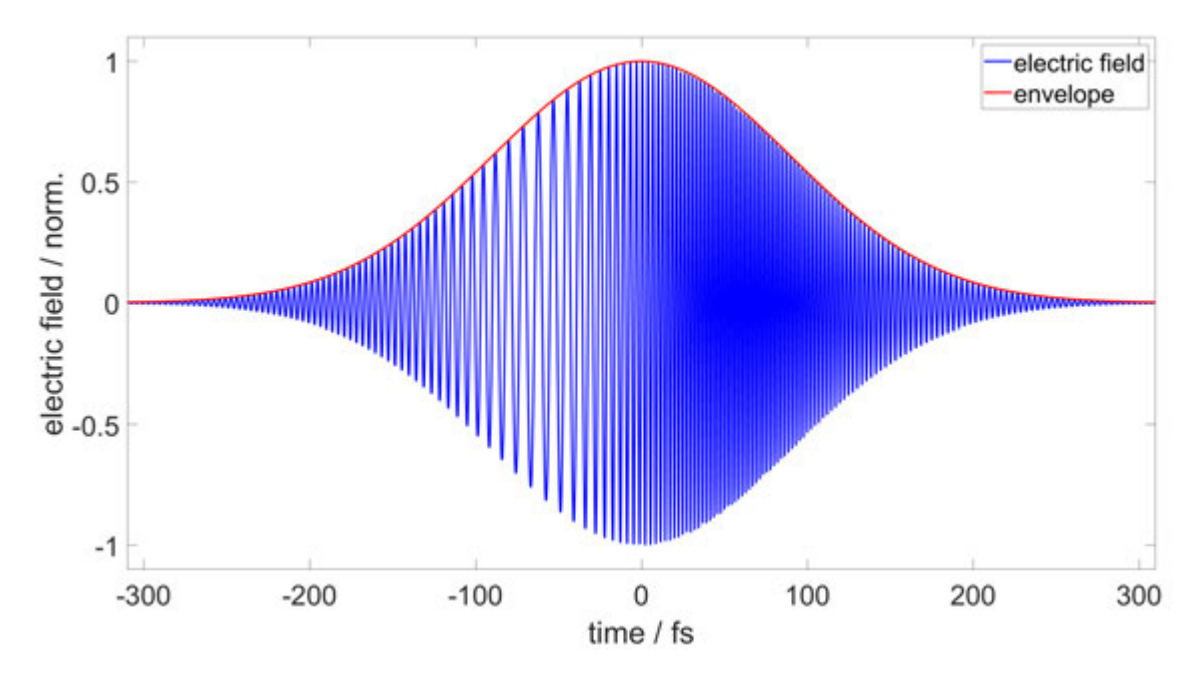


Figure 4: The self phase modulated electric field of the field shown in Figure 1.

2.4 Achieving Large Spectral Broadening

For spectral broadening, waveguides are a good choice since they maintain a pulse's beam size and intensity over a large distance. Additionally, the peak power must remain below the critical power for self-focusing P_{crit} , and the peak intensity must stay below the ionization threshold of the nonlinear medium.

By looking at Equation (9) one can see that to avoid self focusing, it is necessary to limit the refractive index n_0 or the nonlinear refractive index n_2 in order to increase P_{crit} , since the laser wavelength λ is fixed by the laser it self.

$$P_{crit} = \frac{1}{2\pi} \cdot \frac{\lambda^2}{n_0 n_2} \tag{9}$$

There are different definitions for P_{crit} , varying by a constant factor. For simplicity this formula was chosen. By taking Equation 10 into account, it becomes evident that, to prevent ionization as the input peak power P_0 increases, the effective mode area A_{eff} must also be increased, ensuring that the ionization threshold intensity $I_{threshold}$ satisfies the following inequality:

$$I_0 = \frac{P_0}{A_{eff}} \tag{10}$$

$$A_{eff} > \frac{P_0}{I_{threshold}} \tag{11}$$

As a nonlinear medium, in many cases gases are a good choice because of their high damage threshold. Besides that they posses two rather easy changeable quantities to tune the broadening: Firstly the propagation length in the nonlinear medium influences the instantaneous frequency variation, as can be taken from Equation (8). Secondly the gas pressure. The nonlinearity of the refractive index n_2 of the gas is linearly proportional to the gas pressure p. κ_2 represents the proportionality constant. Thus: the nonlinear refractive index becomes tuneable: [7]

$$n_2 = \kappa_2 \cdot p \tag{12}$$

 n_2 is material dependent. For example, air has a nonlinear refractive index $n_{2air} = (5.7 \pm 2.5) \frac{\text{cm}^2}{\text{W}}$ at 1 bar. Compared to that Argon, has a bigger nonlinear refractive index $n_{2Ar} = (19.4 \pm 1.9) \frac{\text{cm}^2}{\text{W}}$ and Neon has a smaller nonlinear refractive index $n_{2Ne} = (1.8 \pm 1.5) \frac{\text{cm}^2}{\text{W}}$. [1] In our case, we decided to use Neon, because of its higher ionization energy of 21.6 eV [3] compared to the ionization energy of Argon of around 15.8 eV. [11]

In hollow core fibers, guiding relies on grazing-incidence reflections. Therefore, the losses increase rapidly when a fiber is bent. The transmission T of a hollow core fiber can be described using Beer's law, with the parameters α representing the losses and L the propagation length. [7]

$$T = e^{-\alpha L} \tag{13}$$

 α can be written in terms of the losses a perfectly straight hollow core fiber would have, α_0 , and the losses due to bending of the fiber α_R .

$$\alpha = \alpha_0 + \alpha_R, \quad \alpha_0 \propto \frac{\lambda^2}{a^3}, \quad \alpha_R \propto \frac{1}{\alpha_0 R^2}$$
 (14)

 α_0 scales with the laser wavelength λ and the inner radius of the fiber a. By increasing a the transmission increases, however also α_R increases and thus making the fibers sensitive to bending. Thus, it is necessary to put normal hollow core fibers on a precisely straight machined V-groove. For flexible hollow core fibers, with walls of a few microns, it is possible to fix the fiber at both

ends and stretch it to straighten it. Similar to the famous catenary problem, that describes a chain fixed at the ends sagging due to gravity to lower its potential energy, the fiber is sagging. The solution for this problem is be a hyperbolic cosine function:

$$z = R\cosh\left(\frac{x}{R}\right) \tag{15}$$

With the minimum radius of curvature R in the middle of the fiber, as can be taken from Figure 5 and the horizontal and vertical coordinates x and z. Since the forces stretching the fiber $F_1 = F_2 = F$ the minimum radius of curvature can be expressed as $R = \frac{F \cdot l}{F_{grav}}$.

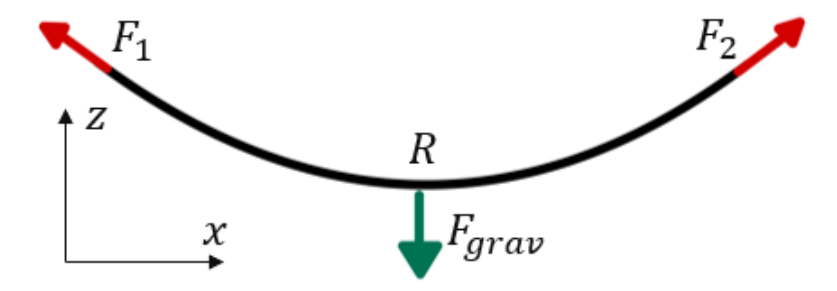


Figure 5: The fiber is fixed at the two ends. R represents the minimum radius of curvature in the middle of the fiber. The red arrows show the forces for stretching the fiber $F_1 = F_2$. The gravitational force F_{qrav} is represented by the green arrow.

Due to the small weight per meter of a few grams or even less, the minimum radius of curvature of a hollow core fiber can be several kilometers with just moderate forces applied for stretching the fiber. [7]

3 Compressor Construction

Realizing a stretched fiber pulse compressor requires three main components: the fiber itself, which is commercially available in 10-m long pieces and must be cut to length, a mechanism to stretch the fiber, and a pressure vessel to fill the fiber with pressured gas.

3.1 Used Fibers

Two types of fibers with different outer diameters were used:

- Fiber I: molex TSP250794, inner diameter $(250 \pm 6) \mu m$, outer diameter $(794 \pm 12) \mu m$ [6]
- Fiber II: molex TSG250350, inner diameter (250 \pm 6) μm , outer diameter (350 \pm 15) μm [6]

3.2 Cutting the Fiber

Even though the fiber can be cut with most types of blades, such as razor blades and scissors, a close up of the interface in Figure 6 reveals that the fiber breaks into two rather than being cut cleanly. Cutting the fiber with special scissors for optic internet cables did not yield better results. The best results came from using a ruby blade to incise the fiber when under tension until it breaks. A photograph of the interface of the thinner fiber, which was taken with a reflected light

microscope, can be seen in Figure 7. Removing the Kapton coating on the outside of the fiber with heat did not improve the cutting, but yielded a brittle fiber.

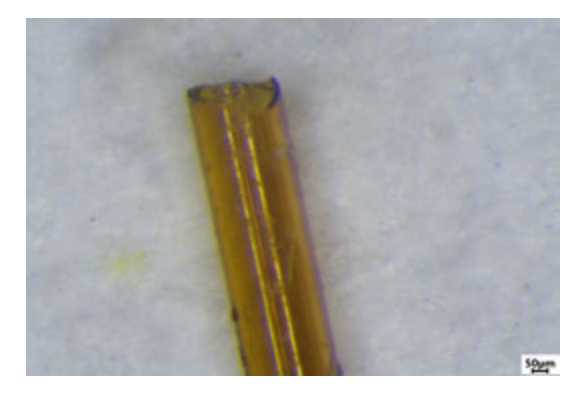


Figure 6: Interface of the thinner fiber, cut with scissors with no tension applied to the fiber.

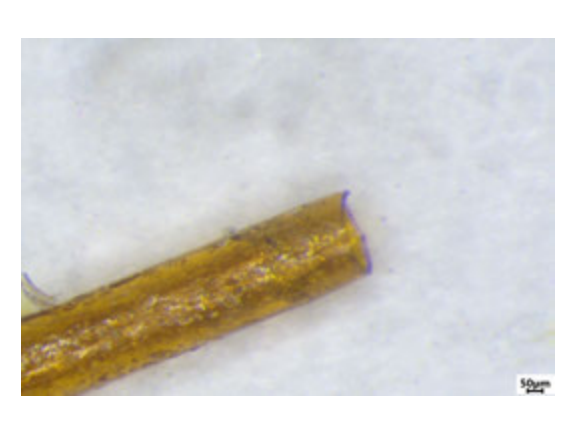


Figure 7: Interface of the thinner fiber, cut with a ruby blade with no tension applied.

Cutting the thicker fiber delivered much cleaner interfaces. Figure 8 is a picture of the fiber taken with the microscope, used to align the setup for full compressor tests. To protect the adhesive joint, a reflector was mounted on the front side of the aluminum profile.



Figure 8: Interface of the thicker fiber, cut under tension with a ruby blade. The picture was taken during the alignment of the laser with the long working distance microscope.

3.3 Mounting the Fiber

It is indispensable that the fiber ends are aligned as straight as possible before fixation, because bending excites high-order modes and causes losses in the fiber. We pursued three alignment approaches before achieving an acceptable transmission mode, which will be detailed briefly:

Hanging Mounting

The first approach to ensure fiber alignment was to glue a flange with a $0.4~\mathrm{mm}$ -diameter hole around the fiber while it was hung vertically. Afterwards the fiber was rotated by 180° and another flange was attached. Figure 9 shows such an early approach of mounting the fiber. This approach did not deliver satisfying results, see 3.4.



Figure 9: Mounting the fiber to the flanges while hanging vertically.

Horizontal, Tensioned Mounting

The second approach was to glue the fiber to two endpoints while being oriented horizontally. One of those endpoints was mounted on a stage, which made it possible to stretch the fiber like a clothing line between the points. The flanges were threaded onto the fiber beforehand and were glued to the tensioned fiber. When the glue hardened, the two ends of the fiber were clipped, so that just the fiber between the flanges was left. This approach did improve the results slightly, see 3.4.

Horizontal, Tensioned Mounting in an Extruded Profile

The final way of mounting the fiber worked: the fiber was again mounted vertically between two endpoints. Differing from the previous approach, we threaded an extruded aluminum profile onto the fiber. The fiber was stretched again using the stage. Then, the profile was moved to center the fiber. Pouring glue into holes at each end of the profile created an adhesive joint between the fiber and the profile, as can be seen in Figure 10 and 11. An additional hole released encapsulated air inside the profile when the pressure vessel was evacuated and filled with Ne.



Figure 10: Mounting the fiber under tension to the aluminum profile: On the left side the fiber was glued to an aluminum stand mounted on the stage. On the right side it was fixed onto a static stand.

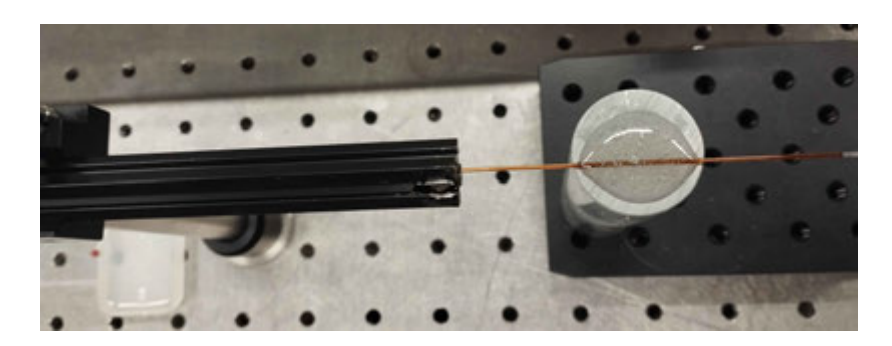


Figure 11: Fixation of the fiber to the aluminum stand shown in Figure 10. As mentioned, the fiber was aligned and glued to the profile by pouring glue into dedicated holes, which can be seen next to the end of the item profile.

3.4 Fiber Coupling Tests (HeNe-Laser)

To judge the quality of the fiber mounting, and predict the coupling and transmission properties of the stretched fibers, we coupled a Uniphase 1108 Helium Neon laser with a wavelength of 633 nm through the fiber. To obtain an impression of the output mode, we first used 30 cm long fibers. To match the fiber core diameter, we increased the laser beam size by a lens and then focused it onto the fiber entrance using another lens. A camera placed in the focal plane was used to ensure a proper beam waist radius. To ensure collinear alignment of the laser and the fiber, we marked a target on a projection screen and adjusted the position and direction of the laser beam using two silver mirrors. Figures 12 and 13 depict the experimental setup.

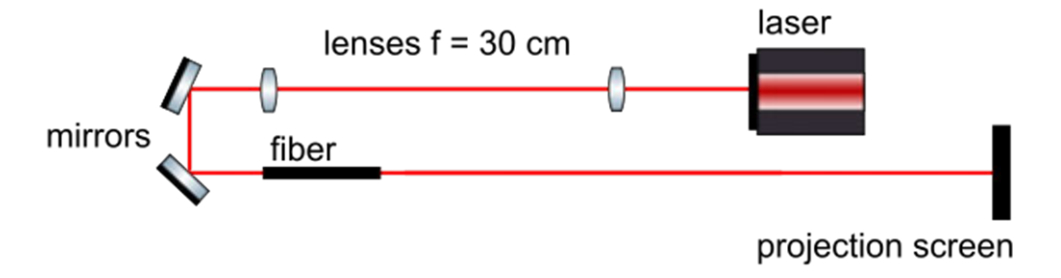


Figure 12: Setup for testing the stretched fibers: The laser propagates through the first lens and is widened, before being again focused by another similar lens. Via two mirrors, the laser is redirected and coupled into the fiber.

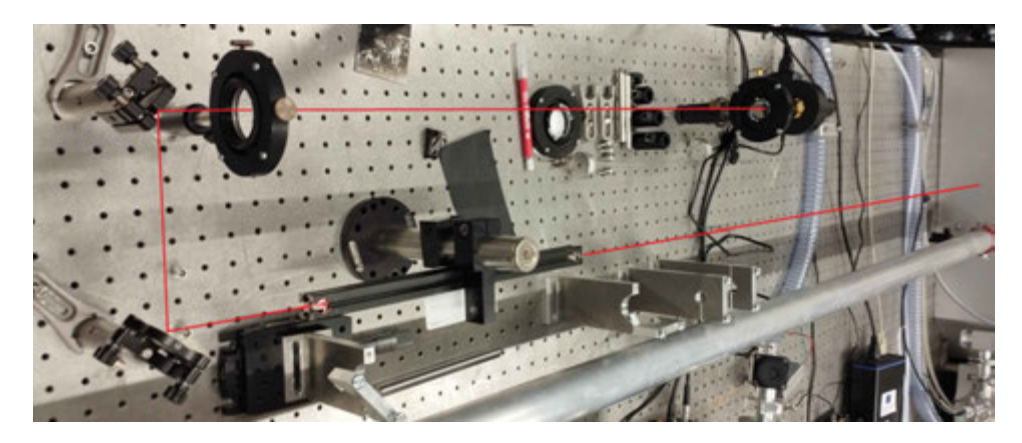


Figure 13: Setup for testing the stretched fibers (compare with the schematic drawing in Figure 12).

Figure 14 documents the progress in achieving a good transmission mode using the different mounting mechanisms. During the first attempt, no round fiber mode was visible. The second test with a horizontally mounted fiber already yielded a transmission mode with the expected spatial structure. The undesired light around the central mode was minimized by properly aligning the setup. However, the best achievable mode was still unsatisfactory. The final test with the fiber glued to an extruded profile almost immediately delivered a fundamental fiber mode.

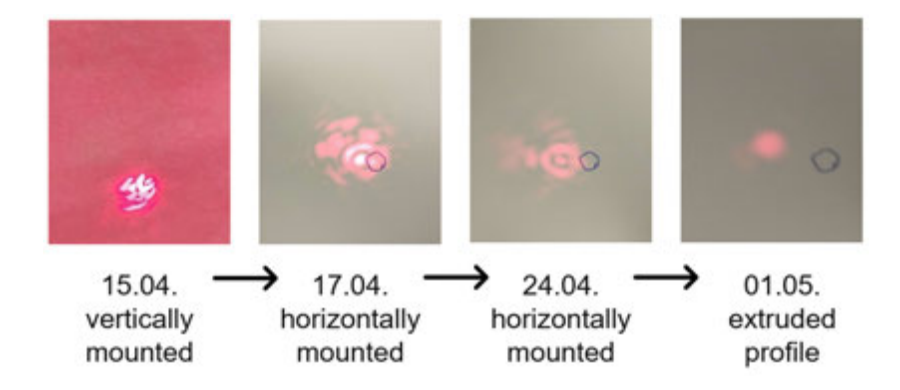


Figure 14: The obtained fiber modes at the projection screen during the optimization of the fiber mounting process.

3.5 Pressure Vessel

To withstand high pressures, the pressure vessel was mainly constructed from stainless steel CF16 components. The laser parameters of the design were chosen similar to an already existing and operational hollow core fiber pulse compressor at the Institute for Experimental Physics constructed by Hana Hampel and [4], to allow parallel testing and operation. Originally, we intended to stretch the fiber between two separated end pieces, which can be seen in Figure 15. However mounting the fiber in an aluminum profile gave better results. This second approach, which can be seen in Figure 16, required a connection of the two end pieces via a tube to fit in the profile, which also replaced the complicated mounting of the fiber using thin holes of around 0.4 mm which had to be drilled through around 1 mm of steel for mounting the fiber as previously described in Chapter 3.3. The production process for drilling the holes proved to be challenging, as the thin drills frequently broke. Additionally, the sensitive fiber is now better shielded from environmental factors and only one connection to the gas supply and the pump is necessary.



Figure 15: Design 1: Two separate pressure vessels are linked by the fiber represented by the blue line. The left side vessel shows a sectional view. The fiber entrance at the right was positioned underneath a upwards pointing viewport. Via a window in this flange, it was possible to monitor if the laser was aimed directly on the fiber via a CMOS Camera.



Figure 16: Design 2: The laser enters the fiber from the right and hits the fiber entrance in the center of the cross-shaped part. The tube pointing upwards connects to the vacuum pump and the gas supply.

The beam enters and leaves the vessel through two windows which are aligned in the Brewster angle to increase transmission (Brewster angle $\theta_B = 56.374^{\circ}$ for BK7 glass at a wavelength of $\lambda = 1030$ nm [10]). Each window has a larger diameter than the actual opening to glue it to the inside of the vessel. The high pressure presses the windows firmly against the vessel wall; the glue's primary function is to hold the window in position and seal the gap between the flange and the window. For mounting the windows, the same compound adhesives from UHU were used as for mounting the fibers. If the laser is focused properly, it reaches high enough power densities to melt and evaporate glass. To avoid damage to the entrance window, it is placed around 45 cm upstream of the focal plane. This distance proved to be enough in the existing compressor setup. To enhance the coupling efficiency, the beam waist radius w_0 must fit to the bore radius a of the fiber. The ideal beam waist radius can be approximated using formula (16). [7]

$$w_0 \approx 0.64 \cdot a \tag{16}$$

This yields an ideal beam waist diameter of $160~\mu m$ for a bore diameter of $250~\mu m$. We use a lens with focal length of f=75~cm to achieve this diameter and couple light into the fiber. To check the beam waist of the laser, the online tool Laser Spot Size Calculator was used to calculate the laser beam diameter in the focal plane. With the given focal length, central wavelength, a beam diameter at the lens of 5.5~mm and a beam quality of 1.1~fm for the laser, a spot size in the focus with a diameter of $197~\mu m$ was obtained. [8] Despite the small discrepancy between the ideal beam diameter and the calculated one, the setup was maintained because it's working with the other compressor.

Safety Considerations

Because of the pressure of up to 25 bar applied to the vessel, the windows have to withstand a stress of up to around 250 $\frac{N}{cm^2}$. To ensure that the vessel will not explode, the window thickness was calculated using the following Equation:

$$t = d \cdot \sqrt{\frac{SF \cdot K \cdot p}{4 \cdot F_a}} \tag{17}$$

Where t is the thickness of the window, d the unsupported diameter of the window, SF the safety factor, K an empirical constant, p the pressure difference between the inside and the outside of the vessel and F_a the apparent elastic limit of rupture modulus. The safety factor SF needs to be chosen carefully to avoid plastic deformation of the material. The maximum stress applied to the window should be smaller by the safety factor SF than F_a . If the window is clamped at the edges, K=0.75 is suitable and if a different mounting without clamping, like gluing, is used, K increases to K=1.125. A pressure of p=25 bar, d=12 mm, SF=2 and an apparent elastic limit of $F_a=63.5$ MPa for BK7 glass yields a thickness of $t\approx 1.79$ mm. Actually used were BK7 glasses with a thickness of t=2 mm from Eksma Optics and a thickness of t=3 mm from Pfeiffer Vacuum. [5]

Leak Testing

To ensure that the pressure vessel is sealed, a leak detection via a Helium leak tester was performed. Such a He leak tester consists in general of two parts: A vacuum pump connected to a gas detector and a gas bottle filled with Helium. The procedure begins by connecting the vacuum pump to the vessel. The pump evacuates the vessel, creating a lower pressure environment that allows any potential leaks to draw in gas. Helium, due to its small atomic size, can easily penetrate through the smallest leaks. Near potential leak points, Helium is released out of the gas bottle and detected if there is a leak. The procedure revealed multiple leaks that were fixed by new gaskets and regluing of the windows

4 Compressor Commissioning

Because of the existing compressor, we had to redirect the beam using two mirrors. To ensure that the laser beam was parallel to the optical table, we used two iris diaphragms at the same height, positioned 3 m apart. One of them was close to the mirrors for aligning the laser, and the other was at the end of the pressure vessel, so that, if we managed to couple through both of them, the laser would be aligned. Again, we used two mirrors to move the laser horizontally and vertically. An additional difficulty was that the laser is operating at 1030 nm, which is not visible. To make the laser visible, we used laser viewing cards coated with a fluorescent material and an infrared viewer. We then set up the fiber without the entrance and exit windows to couple the laser through the fiber. To precisely tune the position of the focal point at the fiber entrance, we placed the focusing lens on a stage and set up a long working distance microscope connected to a monitor to get a realtime image of the laser hitting the fiber. To align for maximum coupling efficiency, we used a power meter with a thermal intensity sensor and a photo diode connected to an oscilloscope. The response time of the photo diode is much faster, revealing changes of the power coupled through the fiber in real time, however the price to pay was that we could just measure the reflection of the laser from an ND-filter. The high intensity of the laser otherwise would saturate the diode. After attaching the entrance and exit window to the setup we had to realign the laser due to a beam offset the laser gets when propagating through the Brewster-angled glass. What followed was the evacuation of the pressure vessel with a rotary vane pump and flushing the vessel twice with Neon. The full setup can be seen in Figure 17. Figure 18 is a picture of the beam line in front of the entrance window. Figure 19 shows the complete pressure vessel integrated in the beam line.

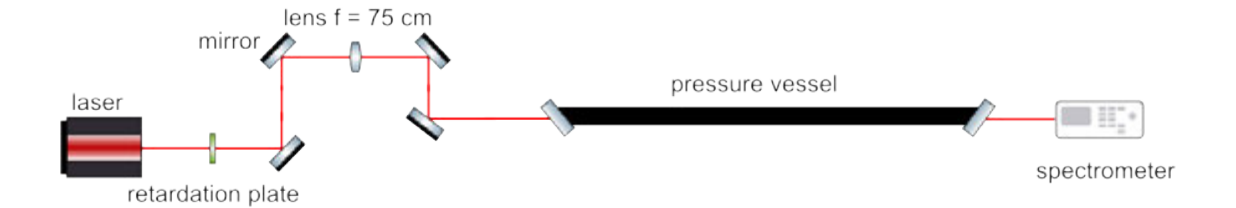


Figure 17: The beam line for the full compressor test: The laser is redirected by the first two mirrors, propagates through the lens mounted on the stage and is redirected into the pressure vessel. At the exit window, we put the photo diode, power meter, and spectrometer.

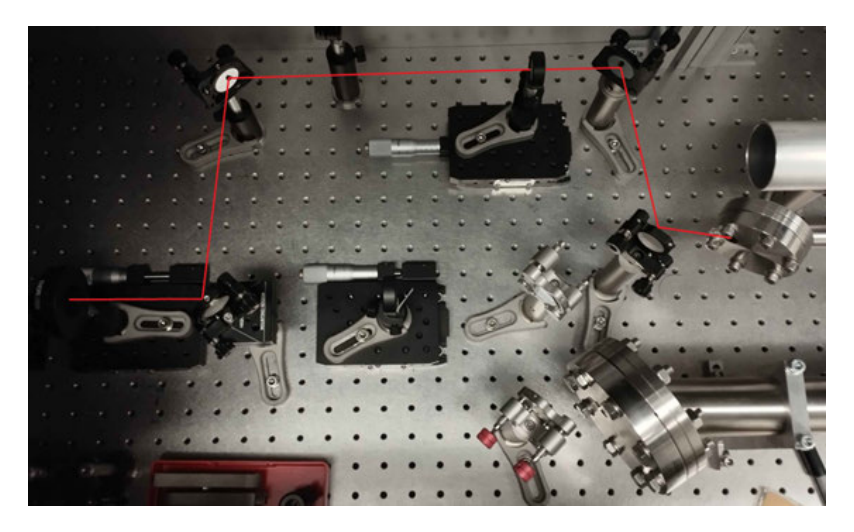


Figure 18: The beam line in front of the entrance window: The laser, represented by the red line, propagates from the left to the right. The first two mirrors only served the purpose of redirecting the beam around the other compressor in the bottom right corner. After propagating through the lens, the laser is again redirected by the two mirrors to couple to the fiber.



Figure 19: In the upper portion of this image, the vessel housing of the other compressor is visible. Alongside to it is the stretched hollow-core fiber compressor, contained within a significantly smaller vessel. The upward-pointing pipe serves as the connection to both the gas supply and the vacuum pump. The enclosure on the right-hand side houses the beam line shown in Figure 18.

4.1 Results Fiber I

After each step detailed in Chapter 4, we measured the intensity at both the entrance and exit of the vessel. However, we were unable to achieve spectral broadening of the laser. Upon evacuating the vessel and applying approximately half of the maximum laser power to the fiber, the fiber evaporated, as illustrated in Figure 20. The measured coupling efficiencies are summarized in Table 1.

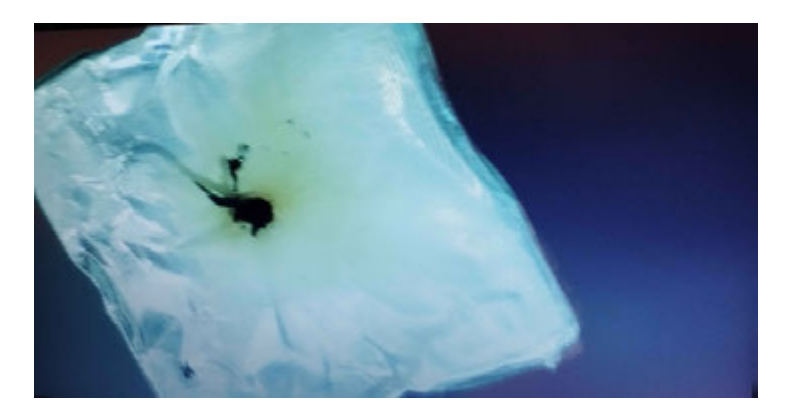


Figure 20: The front face of the profile under the long working distance microscope with the evaporated fiber in the middle after more than 2.74 W hit the entrance.

The cause of the fiber's evaporation was identified by examining the static fiber from the other compressor. As shown in Figure 21, the laser had burned through the glass, resulting in an enlarged bore diameter. This increased bore size was larger than the outer diameter of the stretched fiber, leading to its failure.

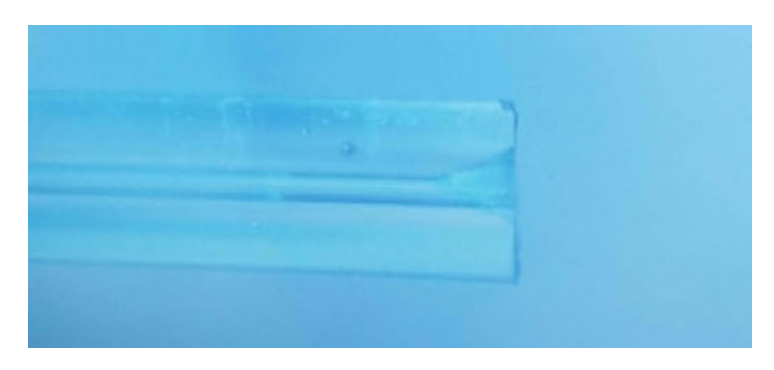


Figure 21: The cone-shaped enlargement of the bore of the static fiber.

Table 1: Measured results for Fiber I: Besides the input power P_{in} and the output power P_{out} , the table contains also the coupling efficiency, the mounted windows and the surrounding atmosphere.

P_{in} / W	P _{out} / W	Efficiency / %	entrance window	exit window	atmosphere
0.83	0.32	38.6	×	×	air
0.06	0.03	50.0	✓	✓	air
0.06	0.04	66.7	✓	✓	vacuum
0.83	0.39	47.0	✓	✓	vacuum
2.74	1.25	45.6	✓	✓	vacuum
>2.74	-	-	✓	✓	vacuum

4.2 Results Fiber II

Using the same setup and alignment procedure with the thicker fiber, we successfully applied full power to the fiber and recorded the data presented in Table 2. Spectra were measured across a pressure range from 0 bar to 21 bar, with increments of 5 bar, using a spectrometer. The resulting spectra are plotted in Figure 22.

For the 16 bar and 21 bar measurements, two spectrometers were used to capture the entire spectral range. This required background light removal and spectral scaling to ensure alignment of the data. Consequently, all other spectral measurements with narrower bandwidths terminate near 900 nm, as shown in Figure 22.

Table 2: Measured results for Fiber II: Besides the input power P_{in} and the output power P_{out} , the table contains also the coupling efficiency, the mounted windows and the surrounding atmosphere. For the last six measurements the corresponding spectrum was measured.

P_{in} / W	P_{out} / W	Efficiency / %	entrance window	exit window	atmosphere
0.86	0.41	47.6	√	×	air
0.86	0.40	46.5	√	✓	vacuum
0.86	0.40	46.5	√	✓	11 bar Neon
3.00	1.29	43.0	√	✓	11 bar Neon
5.47	2.90	53.0	✓	✓	21 bar Neon
5.47	2.70	49.4	\checkmark	✓	16 bar Neon
5.47	2.70	49.4	√	✓	11 bar Neon
5.47	2.80	51.2	√	✓	6 bar Neon
5.47	2.90	53.0	√	✓	1 bar Neon
5.47	3.00	54.9	✓	✓	vacuum

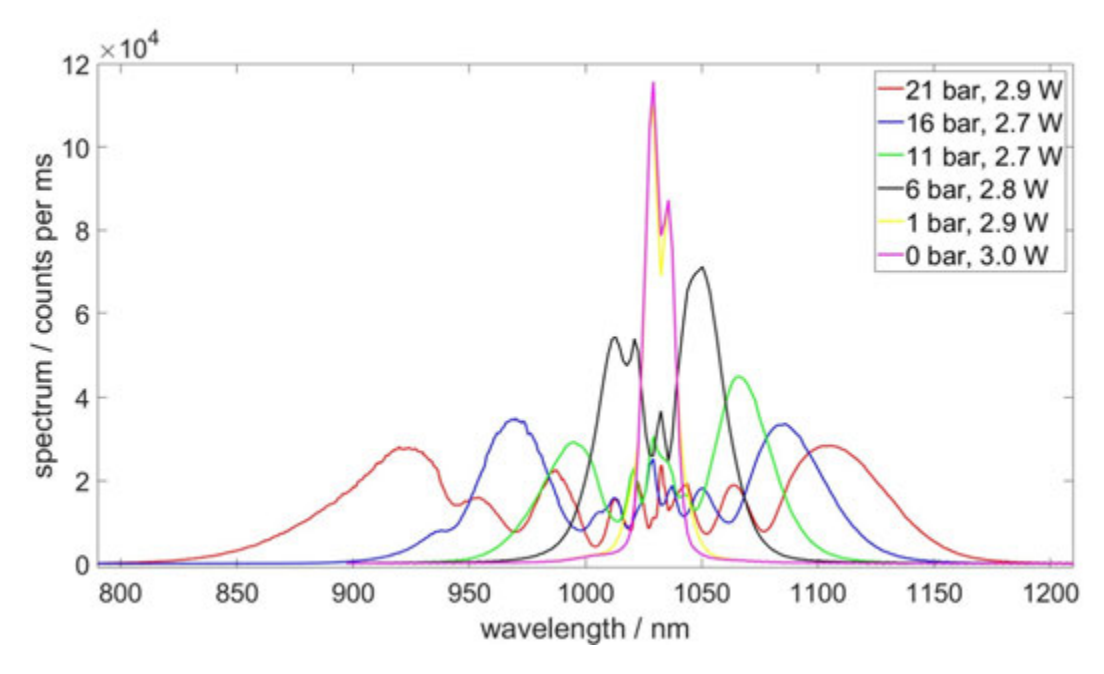


Figure 22: The measured spectra from 0 bar up to 21 bar in steps of 5 bar and their corresponding output power. The input power was held constant at 5.47 W during these measurements.

The pulse duration was not directly measured. However, to estimate the pulse shape in the time

domain and determine its Fourier-limited duration, an inverse Fourier transform of the spectrum shown in Figure 22 was performed. This process involves converting the intensity as a function of wavelength into intensity as a function of frequency. To mitigate the influence of noise, intensity values for wavelengths outside the range of 800 nm to 1200 nm were set to zero, as these regions contained only noise without any significant signal. A two-sided frequency spectrum was then constructed, extending from the negative maximum frequency to the maximum frequency, with two additional points near zero added to prevent duplication of the zero-frequency value. Then, interpolation was applied to create a uniformly spaced frequency array, with intervals determined by the smallest frequency difference, $\Delta\omega_{\rm min}$. Assuming a flat spectral phase, the spectral phase was estimated as the square root of the intensity. After these preparations, the inverse Fourier transformation was executed. The electric field as a function of time (Figure 23) and the intensity as a function of time (Figure 24) were plotted. By measuring the full width at half maximum (FWHM) of the intensity plot, the Fourier-limited pulse duration was determined to be 8.9 fs.

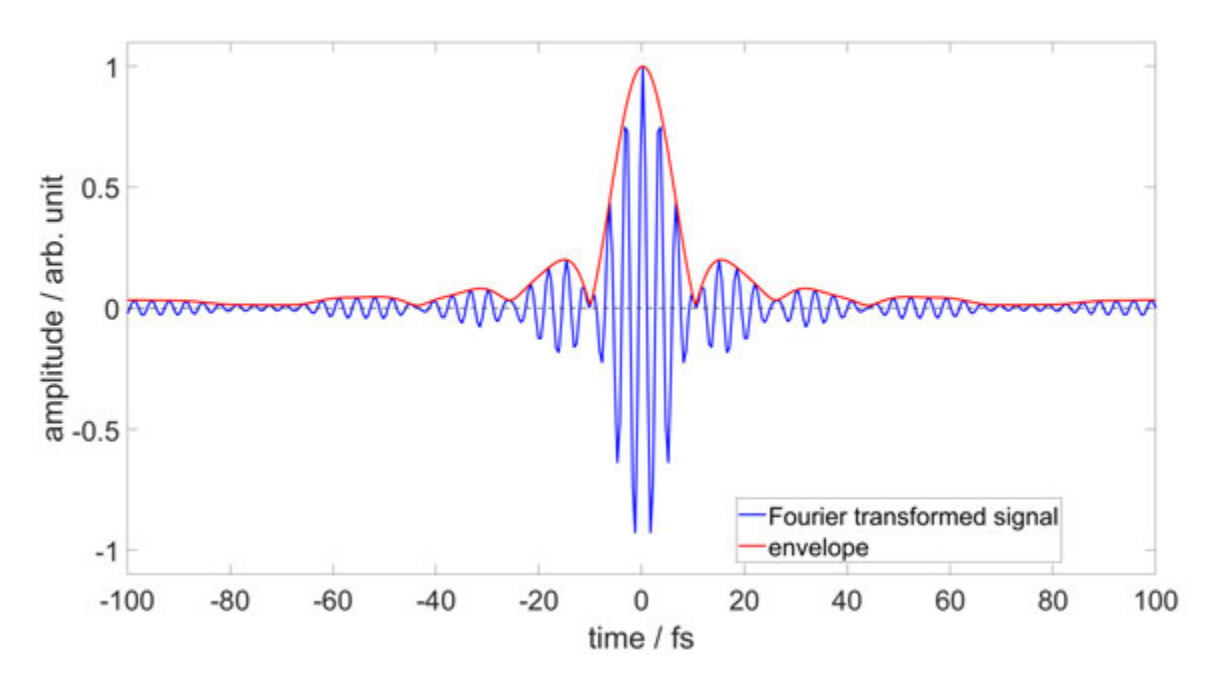


Figure 23: The temporal electric field, obtained from the Fourier transformed spectral amplitude data of the broadened spectrum measured with 21 bar of Ne applied to the vessel.

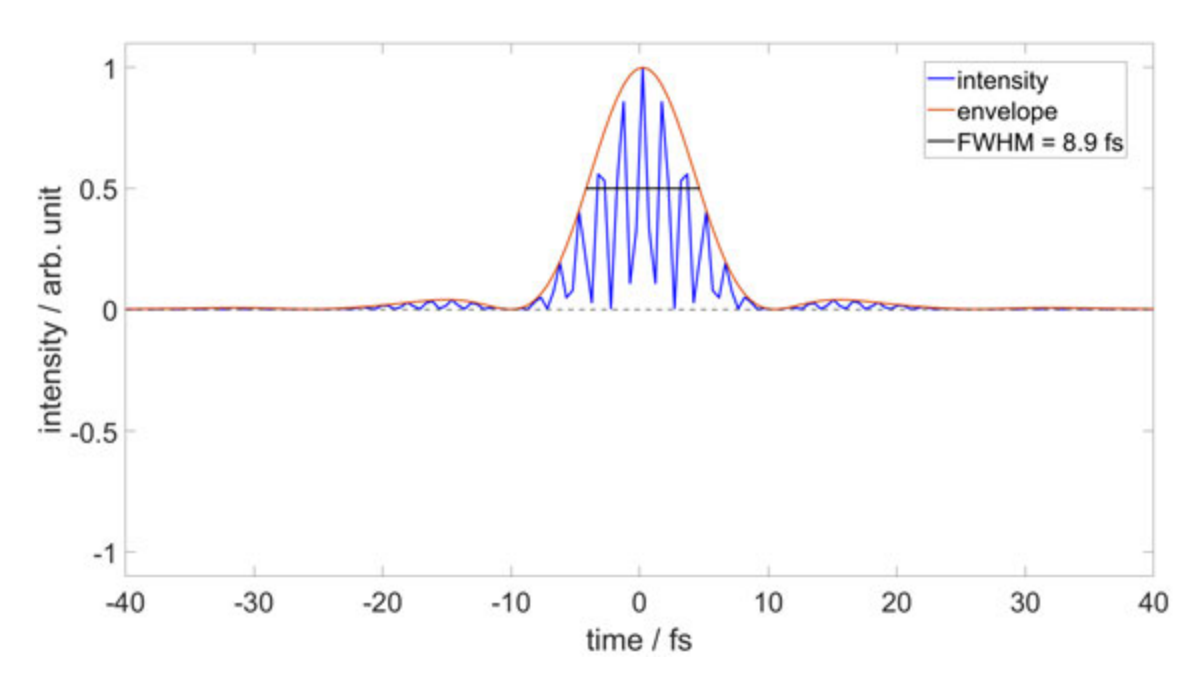


Figure 24: The temporal intensity profile calculated from Figure 23.

5 Discussion and Outlook

We broadened a commercial laser to a spectrum spanning from approximately 830 nm to 1160 nm, with a coupling efficiency of around 55 %. This yielded a Fourier limited pulse duration of around 8.9 fs. In [4], a coupling efficiency of >75 %, a spectral range of 650 nm -1200 nm, and a pulse duration of 8 fs were reached. To achieve comparable results, several enhancements could be made, including replacing the silver mirrors situated in front of the entrance window with mirrors of a higher reflectivity to reduce power loss. An increase in the tension applied to the fiber would, in theory, also deliver better results, but this assumingly would be an insignificant addition. A further step towards achieving enhanced results would be to redesign the entrance and exit windows of the pressure vessel, taking into account the offset of the beam when propagating through the windows themselves or applying a higher gas pressure, which could be increased up to 25 bar with the current windows. Further improvements, which do not affect the quality of compression itself, could be made through the design of an even better reflector to protect the adhesive joint of the fiber. The fiber loses tension immediately when the laser is not aligned properly due to evaporation of the adhesive caused by the heat the laser produces in its focal point. The next step is to retrofit the setup for Argon gas at lower pressure and higher repetition rates using longer fibers with smaller bore radii.

References

- [1] Á. Börzsönyi, Z. Heiner, A. P. Kovács, M. P. Kalashnikov, and K. Osvay. Measurement of pressure dependent nonlinear refractive index of inert gases. *Optics Express*, 18(25):25847–25854, 2010.
- [2] J. C. Diels and W. Rudolph. *Ultrashort Laser Pulse Phenomena: Fundamentals, Techniques, and Applications on a Femtosecond Time Scale*. Optics and Photonics. Academic Press, 1995.
- [3] J. R. Fuhr and W. L. Wiese. *NIST Atomic Transition Probability Tables*. CRC Press, Inc., Boca Raton, FL, 1996.
- [4] E. Goulielmakis H. Y. Kim. Petahertz-scale spectral broadening and few-cycle compression of Yb:KGW laser pulses in a pressurized, gas-filled hollow-core fiber. *Optica Publishing Group*, 47:pp. 5865–5868, 2022.
- [5] Crystran Ltd. The design of pressure windows, 2024.
- [6] Molex. *Polymicro Technologies™ Polyimide Coated Fused Silica Capillary Tubing*. Molex, 2016.
- [7] T. Nagy, P. Simon, and L. Veisz. High-energy few-cycle pulses: post-compression techniques. *Advances in Physics: X*, 6(1):1845795, 2020.
- [8] J. Rissanen. Laser beam spot size calculator. online, 2024. https://www.lasercalculator.com/laser-spot-size-calculator/.
- [9] C. Rullière. Femtosecond Laser Pulses: Principles and Experiments, 2nd Edition. Advanced texts in physics. Springer Science+Business Media, 2005.
- [10] Schott. Optical Glass Datat Sheets. Schott, 2017.
- [11] I. Velchev, W. Hogervorst, and W. Ubachs. Precision VUV Spectroscopy of Ar I at 105 nm. *J. Phys. B*, 32:L511–L516, 1999.